Supporting information

Identifying routes for transferring spin polarization from parahydrogen to protic solvents

Ewoud Vaneeckhaute*[a,b,c], Jean-Max Tyburn[d], James G. Kempf[e], Johan A. Martens[a,b] and Eric Breynaert*[a,b]

a. NMRCoRe, NMR/X-Ray platform for Convergence Research, KULeuven, Celestijnenlaan 200F, box 2461, B-3001 Leuven, Belgium.

b. COK-kat, Centre for Surface Chemistry and Catalysis – Characterisation and Application Team, KULeuven, Celestijnenlaan 200F, box 2461, B-3001, Belgium.

c. Université Claude Bernard Lyon 1, CNRS, ENS Lyon, UCBL, CRMN UMR 5082, 69100 Villeurbanne, France.

d. Bruker Biospin, 34 Rue de l'Industrie BP 10002, 67166 Wissembourg Cedex, France.

e. Bruker Biospin, 15 Fortune Dr., Billerica, 01821 Massachusetts, United States.

Data accessibility: https://doi.org/10.5281/zenodo.13952093

* *Corresponding authors*

Email: eric.breynaert@kuleuven.be

Email: ewoud.vaneeckhaute@kuleuven.be

1. Field cycling hyperpolarization setup

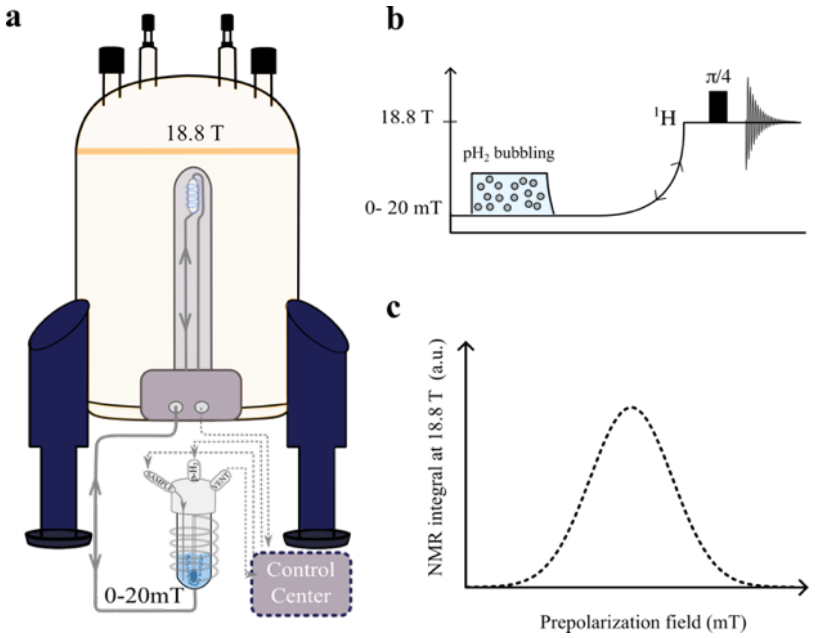

Figure S 1. Field-cycling prototype used to monitor the polarization generated at a pre-polarization field (0-20 mT). A full schematic of the Bruker field-cycling prototype can be found in Figure S1 and S2. b) 90% pH_2 gas at 3 bar is supplied to the mixing chamber underneath the magnet by a pH_2 generator (Bruker, BPHG-90) operating at 37 K. Nitrogen gas is used to field-cycle the SABRE solution to a detection field of 18.8 T (800 MHz). A dedicated flow probe with a 200 µl flow cell allows for measurement of the hyperpolarized signals. c) By repeating the same polarization cycle but varying the pre-polarizing field strengths between 0-20 mT, the polarization transfer field (PTF) profiles in Figure 2 of the main manuscript are constructed.

The field-cycling prototype (Figure S1) contains a control unit (Figure S2a), a low-field mixing chamber (Figure S2b) positioned underneath the spectrometer and a flow probe. The mixing chamber is designed to bubble parahydrogen (pH_2) through a solution containing a transition metal catalyst. The magnetic field in the mixing chamber can be varied from -20 mT to 20 mT using the solenoid coil around (Figure S2b). 90 % pH_2 is supplied by the Bruker ParaHydrogen Generator-90 (BPHG-90) working at 37 K at a maximum output pressure of 10 atm (Figure S2c). The maximum reachable flow rate is 200 cm^3/min (STP). A thermal mixture of hydrogen is supplied by a commercial electrolytic hydrogen generator. In our case 3 bar pH_2 gas is bubbled through 4 mL of a chosen SABRE solution via a glass frit at 295 K and is pneumatically transferred to the detection field in less than two seconds using 5 bar of external nitrogen pressure (from wall or bottle). In this case, the detection happens at 18.8 T in an 800 MHz spectrometer equipped with a $^{1}H/^{13}C/^{29}Si$ flow

probe at 298 K. After detection, the same solution is subsequently returned to the mixing chamber and can be repolarized. PEEK tubing is used transfer the solution between low-field and high-field.

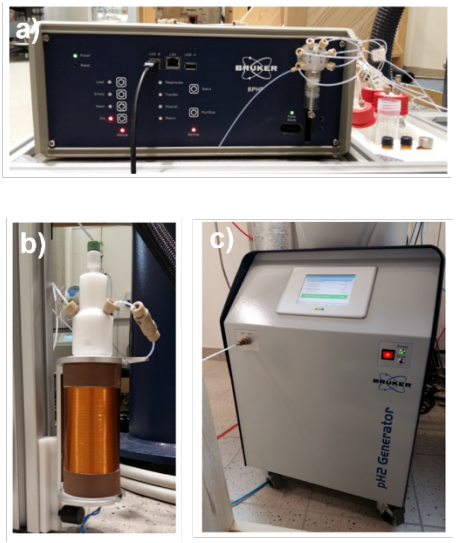

Figure S 2. PHIP hyperpolarization equipment. a) Bruker prototype field cycling control unit, b) a solenoid magnet (approx. −20 to +20 mT) with internal bubbling chamber and c) Bruker pH_2 generator (Bruker, BPHG-90), producing ~90% pH_2 at 37 K. Hydrogen is supplied by an electrolytic hydrogen source producing an ambient thermal mixture of o-H_2 (75 %) and pH_2 (25%) from H_2O.

2. Sample preparation for PTF analysis

A series of four SABRE samples with increasing labile proton concentration [^{1}H] and pyridine and ammonia as coordinating ligand were prepared by dissolving 0.78 mM IrCl(COD)(IMes) **(1a,** the in-house synthesized iridium pre-catalyst[1] with IMes: 1,3-Bis(2,4,6-trimethylphenyl)imidazol-2-ylidene and COD: cyclooctadiene) dissolved in 4 mL CD_3OD (99.97 %, Sigma-Aldrich) (Table S1 and S2). To obtain SABRE mixture **I**, 6 mM pyridine was added to the pre-catalyst solution. To sample **II**, 6 mM pyridine and 100 mM NH_4Cl (powder, Sigma-Aldrich) was added. To sample **III**, 6 mM pyridine and 100 mM $(NH_4)_2CO_3$ (powder, Sigma-Aldrich) was added. To sample **IV**, 170 mM NH_4OH (30 wt% dissolved in H_2O, Sigma-Aldrich) was added without pyridine. Due to the NH_4OH buffer solution an additional 400 mM H_2O was therefore included in sample **IV** as well. The total chemical composition of the catalyst mixtures **I-IV** is summarized in Table S1. After preparation, the SABRE solution was taken up by the syringe pump in Figure S2a and transferred to the mixing chamber in Figure S2b for activation of the pre-catalyst **1a** with 3 bar pH_2 during 10 minutes. Figure S3 shows the general activation pathway for the SABRE catalyst employed. After

every field-cycling study, the system was rinsed with methanol and dried with nitrogen gas to minimize any chemical trace impurities in between field-cycling experiments.

Table S 1. Sample composition of SABRE solutions with mixed pyridine and ammonia ligation. Concentrations are in mM.

	SABRE mixtures			
Components (mM)	**I**	**II**	**III**	**IV**
IrCl(COD)(IMes)	**0.78**	**0.78**	**0.78**	**0.78**
Pyridine	**6**	**6**	**6**	/
NH_4Cl	/	**100**	/	/
$(NH_4)_2CO_3$	/	/	**100**	/
NH_4OH	/	/	/	**170**
H_2O	/	/	/	**400**

Table S2. Labile proton concentrations and protonation degree of each SABRE solution I-IV. The remaining protons in deuterated methanol (99.97% deuteration) is estimated to introduce 80 mM of protons to each solution.

	SABRE mixtures			
Proton/deuteron	**I**	**II**	**III**	**IV**
Total [^{1}H]	**0.08 M**	**0.48 M**	**0.88 M**	**1.73 M**
Total [^{2}H]	**31 M**	**31 M**	**31 M**	**31 M**
Protonation degree	**<0.24 %**	**1.5 %**	**2.8 %**	**5.6 %**

3. Spontaneous ammonia generation

Different ammonium buffers (NH_4Cl, $(NH_4)_2CO_3$, NH_4OH) were used to control the amount of ammonia being generated in protic conditions as reported before in Vaneeckhaute *et al.*[2] The equilibrium concentration of ammonia (NH_3) versus ammonium (NH_4^+) in aqueous or methanol solution can be estimated according to the acid/base equilibrium reaction in both media:

$$NH_3 \; + \; H_2O \rightleftharpoons \; NH_4^+ \; + \; OH^- \qquad \text{pKa} = 9.25 \qquad (1)$$

$$NH_3 \; + \; CH_3OH \; \rightleftharpoons \; NH_4^+ \; + \; CH_3O^- \qquad \text{pKa} = 9.55 \text{ [ref 3]} \qquad (2)$$

Note that the pKa value of the ammonia/ammonium equilibrium changes only slightly in methanol as reported in Rossini *et al.*[3] A calibrated pH meter taking into account the different autoprotolysis constant of methanol ($K_{methanol} = 16.6$) was used to measure the pH values reported in the main manuscript in Figure 1. This way, we can have an estimate of the produced ammonia concentration. Using 100mM NH_4Cl, the measured pH was 6.43 and results in almost no generation of ammonia with respective to a pKa of 9.55. In case of 100 mM $(NH_4)_2CO_3$, the pH rises to 9.11 because the carbonate ion is a stronger conjugated base than the chloride ion. The equilibrium concentration of ammonia rises approximately to 50 mM. Finally with 170 mM NH_4OH, the pH measures 9.64 and corresponds to approximately 85 mM of ammonia.

4. Catalyst configuration elucidation

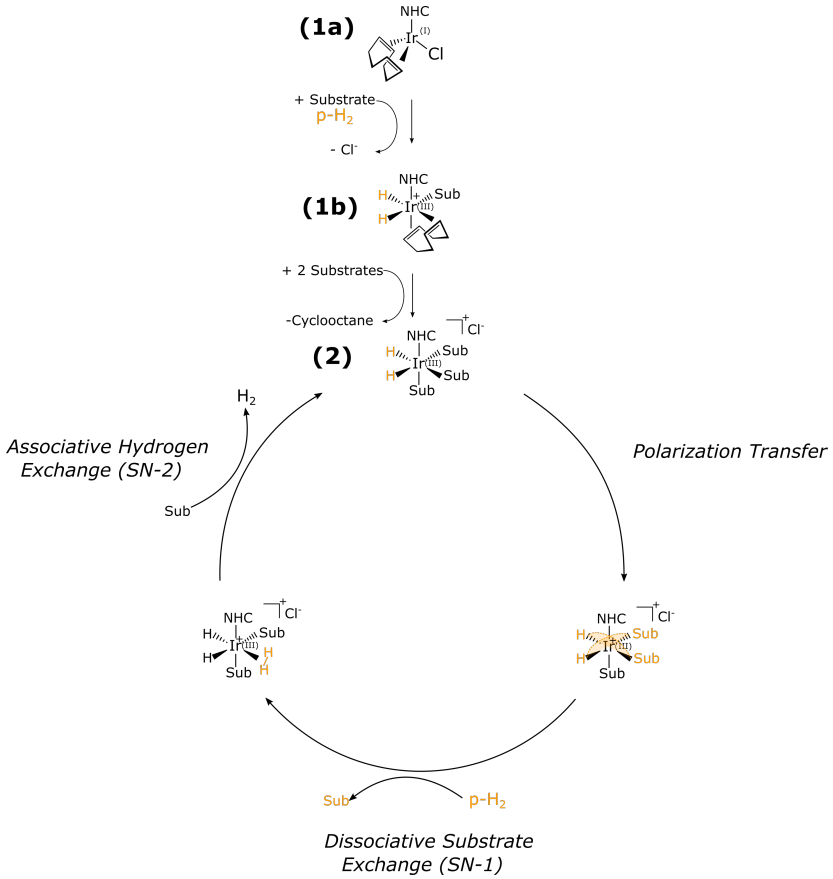

Figure S 3. The general catalytic cycle in case of a SABRE experiment. The substrates are in this case ammonia and pyridine. Activation of the tetrahedral N-Heterocyclic Carbene (NHC) precursor catalyst IrCl(COD)(IMes) (1a) generally results in the $[Ir(IMes)(H_2)(COD)(S_{eq})]Cl^-$ complex (1b) and then transforms in the active octahedral $[Ir(IMes)(H_2)(S_{eq1}S_{eq2}S_{ax})]Cl^-$ complex (2).

The ability to vary the ammonia production in the SABRE solution according to the buffer used is a tool to control the ligation sphere of the active SABRE catalyst.[2] Characterization of stereochemical configurations of the catalyst can be elucidated based on the analysis of isolated proton region between δ = -10 ppm to -25 ppm that correspond to the hydrides from the octahedral complexes in the general form of **1b** and **2**. Specific elucidation of the main catalytic species present when using identical SABRE solutions **I-IV** can be found in Vaneeckhaute *et al.*[2] The hyperpolarized 1D and 2D NMR results of the hydride region are readapted here for clarification and shown in Figure S4 and Figure S5.

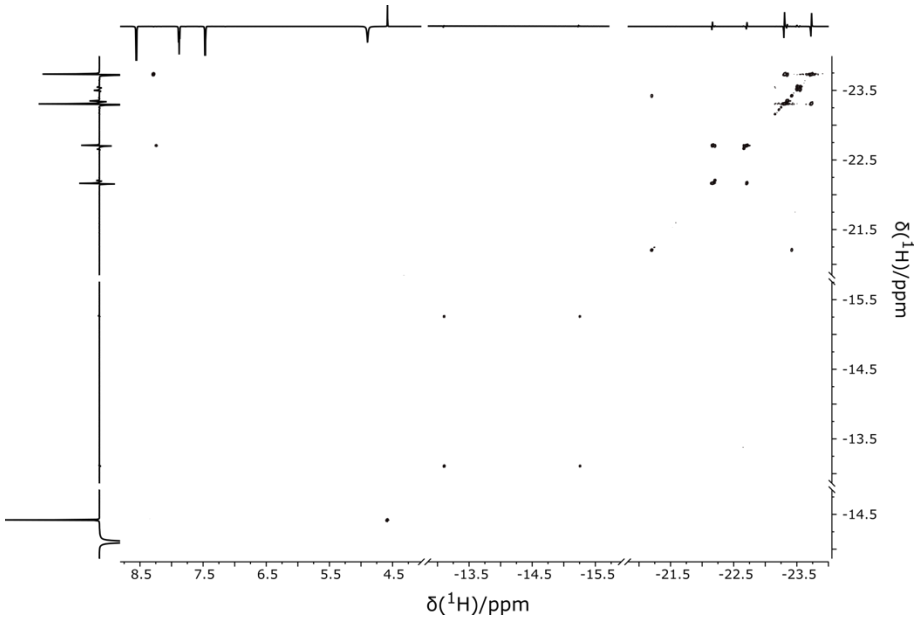

Figure S 4. The full 2D hyperpolarized only parahydrogen spectroscopy (OPSY)[4] COSY plot performed on SABRE mixture III with IrCl(COD)(IMes), pyridine and $(NH_4)_2CO_3$ dissolved in CD_3OD. After a single pH_2 bubbling period of 2 minutes at 6 mT, 1536 transients with sparse sampling of 15% were captured at 800 MHz to construct the 2D plot giving a total of 2.5 min experimental time. The 2D data set was processed using a static NUS reconstruction with TRAF apodization of 1 Hz and zero-filled to 4096 (F1) x 8192 (F2) complex points. Hyperpolarized 1D field cycle measurements were used as external projections accordingly. The cross peaks noticed between hydride resonances at δ = -13.25 ppm and δ = -15.25 ppm are from complex 1b in Figure S3 with ammonia as activating ligand. The cross peaks between δ = -22 ppm and δ = -24 ppm are from mixed-ligand complexes 2b, 2c and 2d shown in Figure S5.

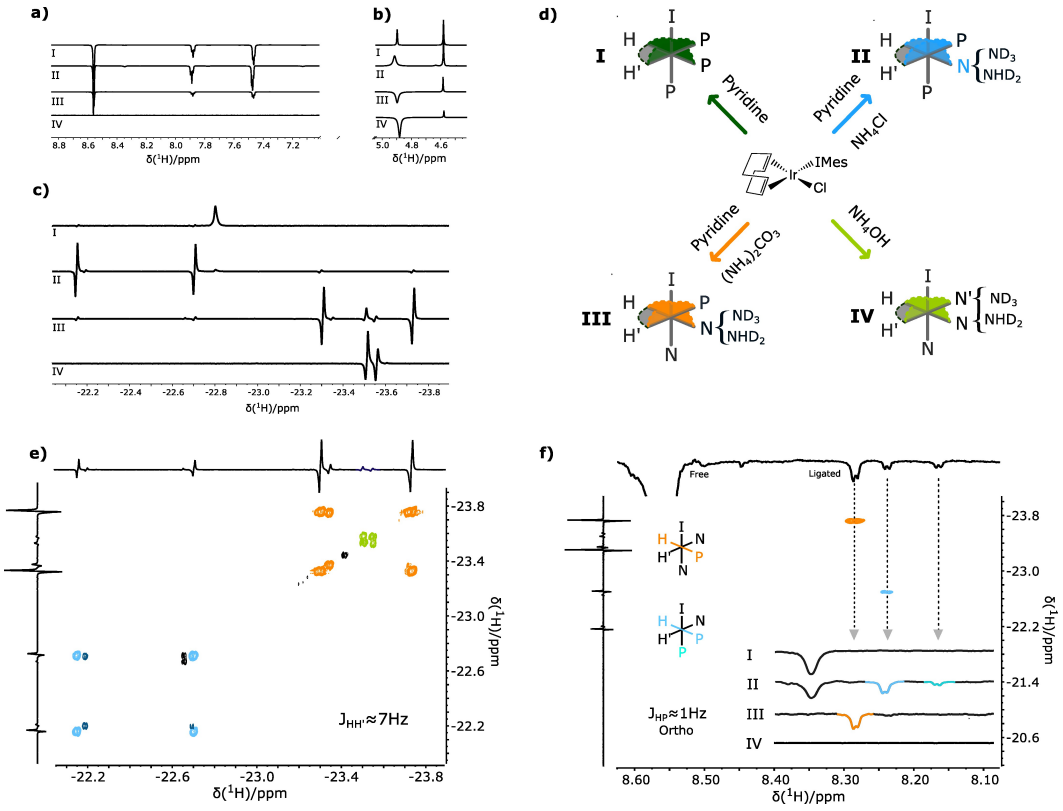

Figure S 5. Characterization of the main catalytic species present in solution by 1D (45° pulse)[5] and 2D ^{1}H NMR (OPSY-COSY)[4] analysis of the hydride region at 800 MHz when preparing SABRE solution I-IV with the chemical composition shown in Table S1. a-c) 1D ^{1}H NMR spectra after a 45° pulse corresponding to SABRE solutions I-IV of a) the pyridine region between 7-9 ppm, b) the o-H_2 (4.58 ppm) and exchangeable proton region (4.9 ppm) and the hydride region between -22 and -24 ppm. The antiphase line shape of the hydride region comes from the longitudinal two-spin order derived from the singlet state of pH_2 after singlet-triplet mixing at high-field.[5] A 45° pulse is required to convert this longitudinal two-spin order into observable but antiphase magnetization. d) The main catalytic complexes 2a, 2b, 2c and 2d present in solution when employing mixtures I-IV. e) 2D OPSY-COSY plot from Figure S4 showing in detail the coupling network of hydrides corresponding to mixed-ligand complexes 2b, 2c and 2d. 2D COSY plot from Figure S4 showing the coupling network of hydrides with ortho-pyridine protons corresponding to mixed-ligand complexes 2b, 2c. The 2D plots are reproduced and readapted from Vaneeckhaute *et al.*[2]

High-field 1D and 2D ^{1}H NMR analysis of the hydride region after pH_2 bubbling at the optimal low-field conditions of 6 mT. Cross-correlation analysis between the hydrides mutually (Figure S5e) and between the hydrides and the ortho protons on ligated pyridine (Figure S5f) have shown before that for SABRE mixtures **I-IV**, the main catalytic species are respectively **2a, 2b, 2c** and **2d**, besides minor contributions of the rest.[2] For example, for mixture **III**, besides the main presence of **2c**, also **2b** and **2d** are noticed. Interpretation of the field-cycling results and the solvent polarization pathways are done considering the main catalytic species present for each mixture. A qualitative estimation of the relative abundance of each catalytic species is possible by comparing the intensity of the hydride signals, similar to the chemo-sensing approach of Tessari *et al.*[6] Note that this holds only for mixed-ligand SABRE catalyst with a large quantity of co-ligand where

spontaneous hydride singlet-triplet mixing is responsible for the hydride intensity. The contribution of catalyst **2a** is therefore presumably underestimated since this is not a mixed-ligand catalyst and spontaneous hydride singlet-triplet mixing does not occur at high-field. In Table S3, the relative contribution for **2a, 2b, 2c** and **2d** is given for each mixture. Occurrence of other catalyst configurations are possible (with counterion Cl- or methanol as a ligand)[7], but due to their short-lived state could not be observed here.

Table S 3. Catalyst composition of SABRE solutions I-IV. A trace amount of ammonia (*) seemed present in solution I from contamination from other field-cycling experiments but is negligible for interpretation of the results.

	SABRE mixtures			
Catalysts configurations (%)	**I**	**II**	**III**	**IV**
2a	**98.6 %**	**1.4 % ***	/	/
2b	**35.14 %**	**64.86 %**	/	/
2c	/	**15.8 %**	**76.4 %**	**7.8 %**
2d	/	/	/	**100%**

5. Polarization transfer field plots

5.1. Mixture I with pyridine

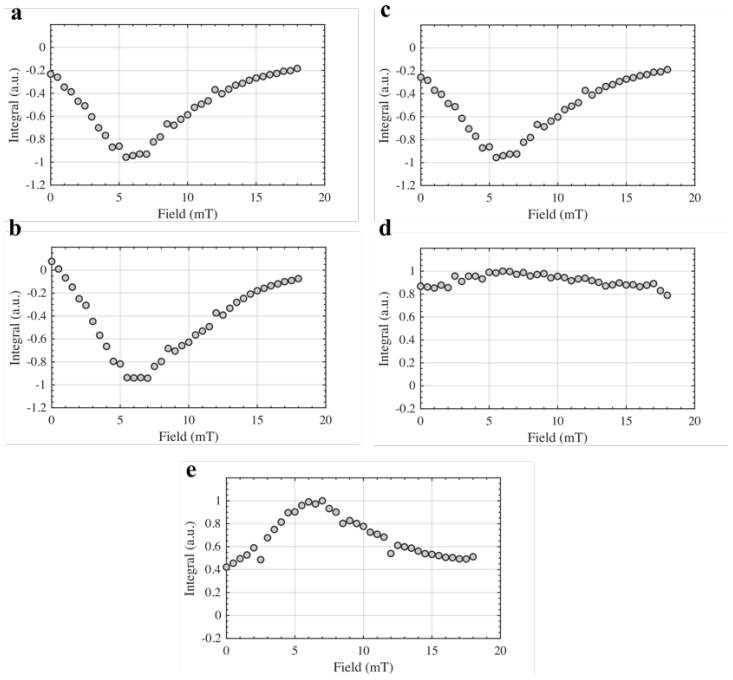

Figure S 6. Normalized polarization transfer field profiles of SABRE mixture I to monitor the influence of the low-field strength (0-20 mT) on the polarization generated by pH_2 in the target protons. A detection field of 18.8 T is used to measure the induced polarization. a) Ortho (7.4 ppm), b) meta (7.8 ppm) and c) para (8.6 ppm) protons of pyridine. d) Hydrogen signal at 4.58 ppm. e) Labile protons of protic solvent (methanol in this case). For construction of the plots, the instrumentation in Figure S2 is used with the pulse sequence in Figure S1b. MATLAB is used for processing the data. The codes are available at https://doi.org/10.5281/zenodo.13952093.

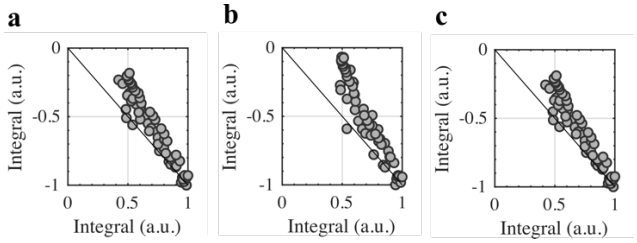

Figure S 7. Correlation plots of mixture I displaying the solvent integral (x-axis) versus the integral of ortho (a), meta (b), and para (c) protons of pyridine (y-axis) at each pre-polarization field strength.

5.2. Mixture II with pyridine and NH_4Cl

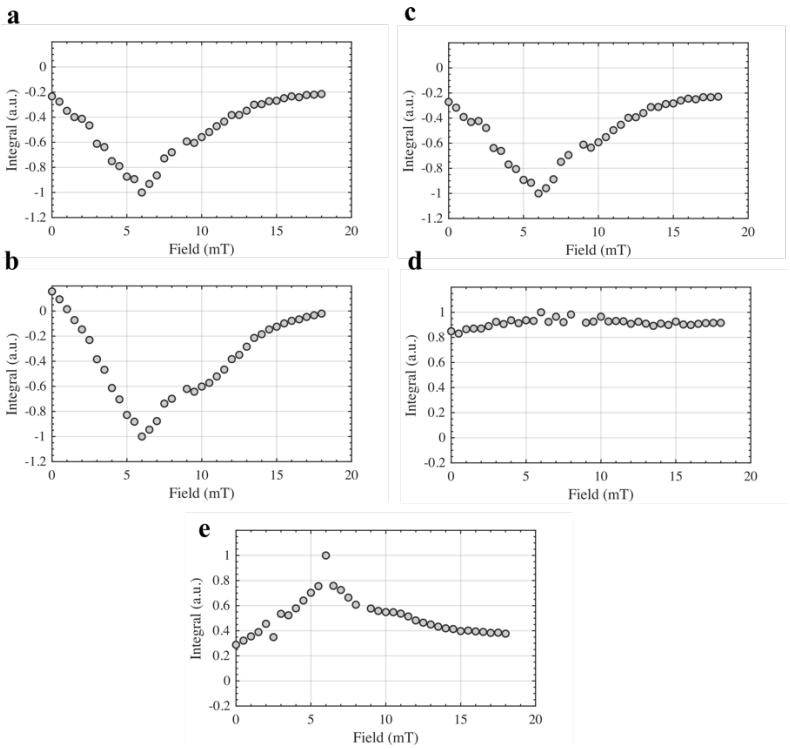

Figure S 8. Normalized polarization transfer field profiles of SABRE mixture II to monitor the influence of the low-field strength (0-20 mT) on the polarization generated by pH_2 in the target protons. A detection field of 18.8 T is used to measure the induced polarization. a) Ortho (7.4 ppm), b) meta (7.8 ppm) and c) para (8.6 ppm) protons of pyridine. d) Hydrogen signal at 4.58 ppm. e) Labile protons of protic solvent (methanol in this case). For construction of the plots, the instrumentation in Figure S2 is used with the pulse sequence in Figure S1b. MATLAB is used for processing the data. The codes are available at https://doi.org/10.5281/zenodo.13952093.

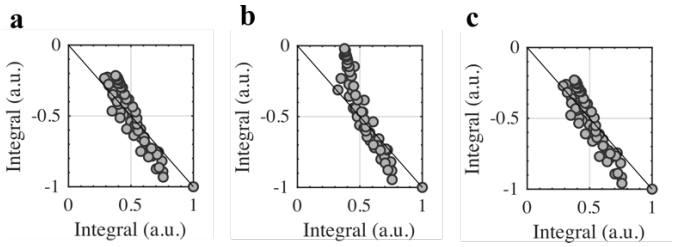

Figure S 9. Correlation plots of mixture II displaying the solvent integral (x-axis) versus the integral of ortho (a), meta (b), and para (c) protons of pyridine (y-axis) at each pre-polarization field strength.

5.3. Mixture III with pyridine and $(NH_4)_2CO_3$

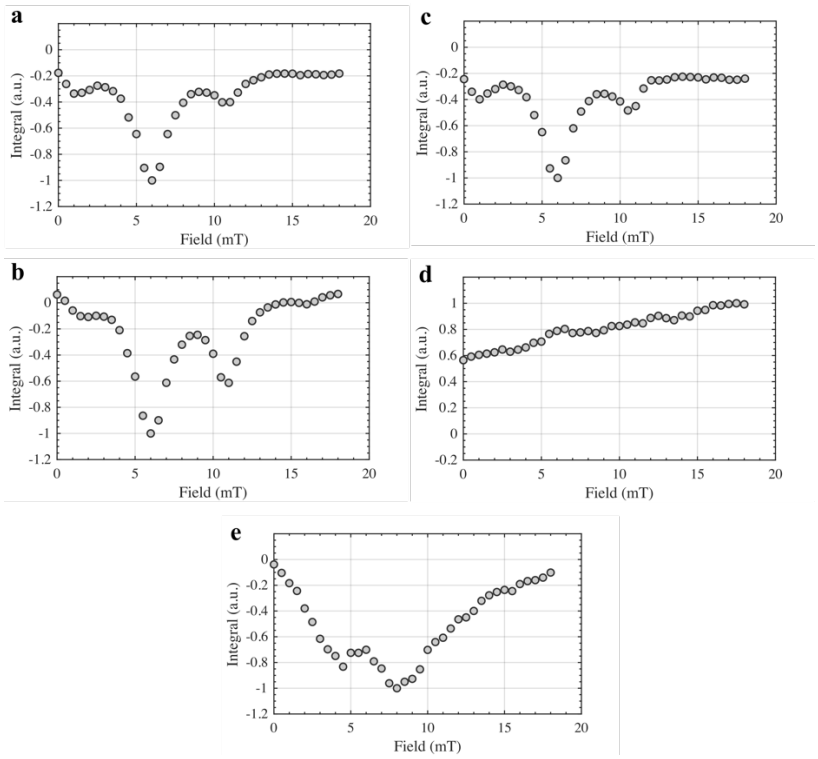

Figure S 10. Normalized polarization transfer field profiles of SABRE mixture III to monitor the influence of the low-field strength (0-20 mT) on the polarization generated by pH_2 in the target protons. A detection field of 18.8 T is used to measure the induced polarization. a) Ortho (7.4 ppm), b) meta (7.8 ppm) and c) para (8.6 ppm) protons of pyridine. d) Hydrogen signal at 4.58 ppm. e) Labile protons of protic solvent (methanol in this case). For construction of the plots, the instrumentation in Figure S2 is used with the pulse sequence in Figure S1b. MATLAB is used for processing the data. The codes are available at https://doi.org/10.5281/zenodo.13952093.

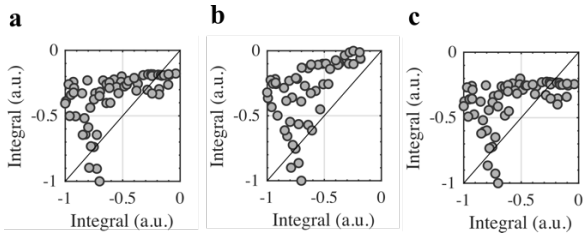

Figure S 11. Correlation plots of mixture I displaying the solvent integral (x-axis) versus the integral of ortho (a), meta (b), and para (c) protons of pyridine (y-axis) at each pre-polarization field strength.

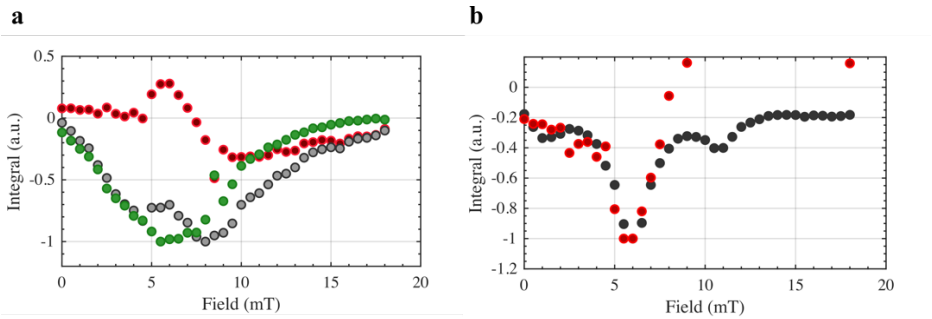

Figure S 12. Decomposition of the solvent pre-polarization field profile in SABRE mixture III (grey, with ammonia and pyridine) using solvent pre-polarization field profile of SABRE mixture IV as a reference (green, with only ammonia). a) The red profile shows the subtraction of the grey solvent field profile (III with pyridine) from the solvent green field profile (IV, without pyridine). An underlying narrow positive contribution to the solvent signal around 6 mT is noticed. b) After normalization and changing the sign, the shape of the red profile seems to correspond to the field profile of the ortho-protons of pyridine shown in black. MATLAB is used for processing the data. The codes are available at https://doi.org/10.5281/zenodo.13952093.

At 6 mT, the dip in negative solvent polarization corresponds with the low-field value where pyridine is hyperpolarized most efficiently as shown in Figure 2i of the main manuscript. The cross-relaxation contribution of pyridine becomes even more clear by subtraction of the solvent PTF profile in Figure 2h from the solvent PTF profile of solution **IV** in Figure 2k where pyridine is omitted, and only ammonium hydroxide is present. The positive solvent contribution is depicted in Figure S12 and corresponds with the position and shape of the sharp maxima of the pyridine protons in Figure 2i.

6. Ammonia isotopologues

6.1. Binomial distribution

Although ammonia's chemical simplicity, a variation in nitrogen isotopologues (ND_3, NHD_2, NH_2D and NH_3) are present after exchange with CD_3OD.[8] An understanding of their relative contribution can be used to rationalize the hyperpolarization of labile solvent protons through ammonia. The presence of protons in ammonia is namely required for transferring hyperpolarization to the protic

solvent. The relative contribution of each nitrogen isotopologue depends on the ratio of protons and deuterons in the solution and follows a binomial distribution according to:

$$x = \binom{n}{k} p^k (1-p)^{n-k}, \tag{3}$$

with x being the relative fraction of each isotopologue, n the total number of isotopologue configurations possible (4 in case of ammonia), k the number of protons specific to each isotopologue and p the ratio of deuterons versus protons in the solution. A visual representation of this distribution in respect to the protonation degree of the solvent is given in Figure S13.

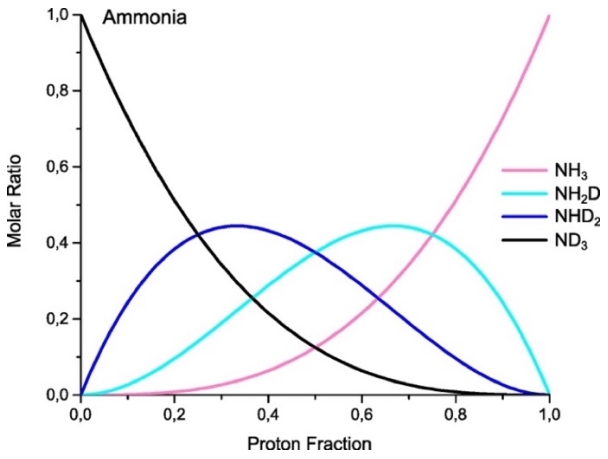

Figure S 13. The molar ratio of ammonia isotopologues in function of the protonation degree of the CD_3OD solvent based on the binomial distribution of equation 3.

In Table S2, the protonation degree of each sample is calculated based on the chemical composition of the SABRE solution in Table S1. Since only a protonation degree of 1.3 % is apparent in the SABRE samples, 95% ammonia will be present as ND_3, and approximately 5 % as NHD_2. The latter will therefore be the main species responsible for the hyperpolarization of the solvent.

6.2. Hydride response to ammonia isotopologues

Normally, fast exchange apparent in protic conditions at basic pH makes isotopologue analysis using ^{1}H-NMR impossible. However as reported recently in our group the contribution of each isotopologues can be observed when ligated to the SABRE catalyst and is reflected in the hydride resonances.[8] Depending on the functional group, spontaneous formation of different nitrogen

isotopologues were noticed to slightly change the chemical shift of the trans positioned hydrides if ligated to the iridium catalyst. In our case, the protons present in the ammonium buffer solutions (see Table S2) already spontaneously generates 5 % NHD_2 for mixture **II** and **III**, while in mixture **IV** this is 20 % NHD_2. This can be seen in the 1D and 2D hydride plots displayed in Figure S5.

7. Reversible solvent hyperpolarization at high proton concentration

Molar polarization, defined as the product of the spin polarization and the concentration of target nuclei, is directly proportional to the NMR signal and therefore a better benchmark for the efficiency of the hyperpolarization method than only the polarization.[9] Here, the ability of parahydrogen together with ammonium buffers to reversibility generate solvent hyperpolarization at low-field (6 mT) in solutions with highly concentrated exchangeable protons (up to 13.3 M) is further explored. The SABRE solutions are based on mixture **IV** (Table S1) where only the aqueous buffer NH_4OH was added to the 0.78 mM of the iridium precursor **1a** (Figure S3) dissolved in 4 mL of CD_3OD. However, the concentration of the buffer solution was elevated to produce [^{1}H] of 6.68 M and 13.28 M for respectively SABRE solutions **IV-VI** in Table S4. The protons originate from water and ammonium. Molar polarization values are calculated using P x [^{1}H] where [^{1}H] is the concentration of labile protons in solution and P is the solvent polarization generated at low-magnetic field. P is calculated by dividing the integrated hyperpolarized solvent signal with the thermal signal at 18.8 T.

Table S 4. Sample composition of SABRE solutions with high concentration of exchangeable protons.

	SABRE mixtures		
Components	**IV**	**V**	**VI**
Ir(Cl)(COD)IMes	**0.78 mM**	**0.78 mM**	**0.78 mM**
NH_4OH	**0.17 M**	**0.68 M**	**1.36 M**
H_2O	**0.4 M**	**1.6 M**	**3.2 M**

Table S5. Total concentration of mobile protons and the overall protonation degree of partially aqueous SABRE solution IV-VI. The remaining protons in deuterated methanol (99.97% deuteration) is estimated to introduce 80 mM of protons to each solution.

	SABRE mixtures		
Proton/deuteron	**I**	**II**	**III**
Total [^{1}H]	**1.73 M**	**6.68 M**	**13.28 M**
Total [^{2}H]	**31 M**	**31 M**	**31 M**
Protonation degree	**5.4 %**	**17.8 %**	**28.4 %**

8. Lifetime of solvent polarization

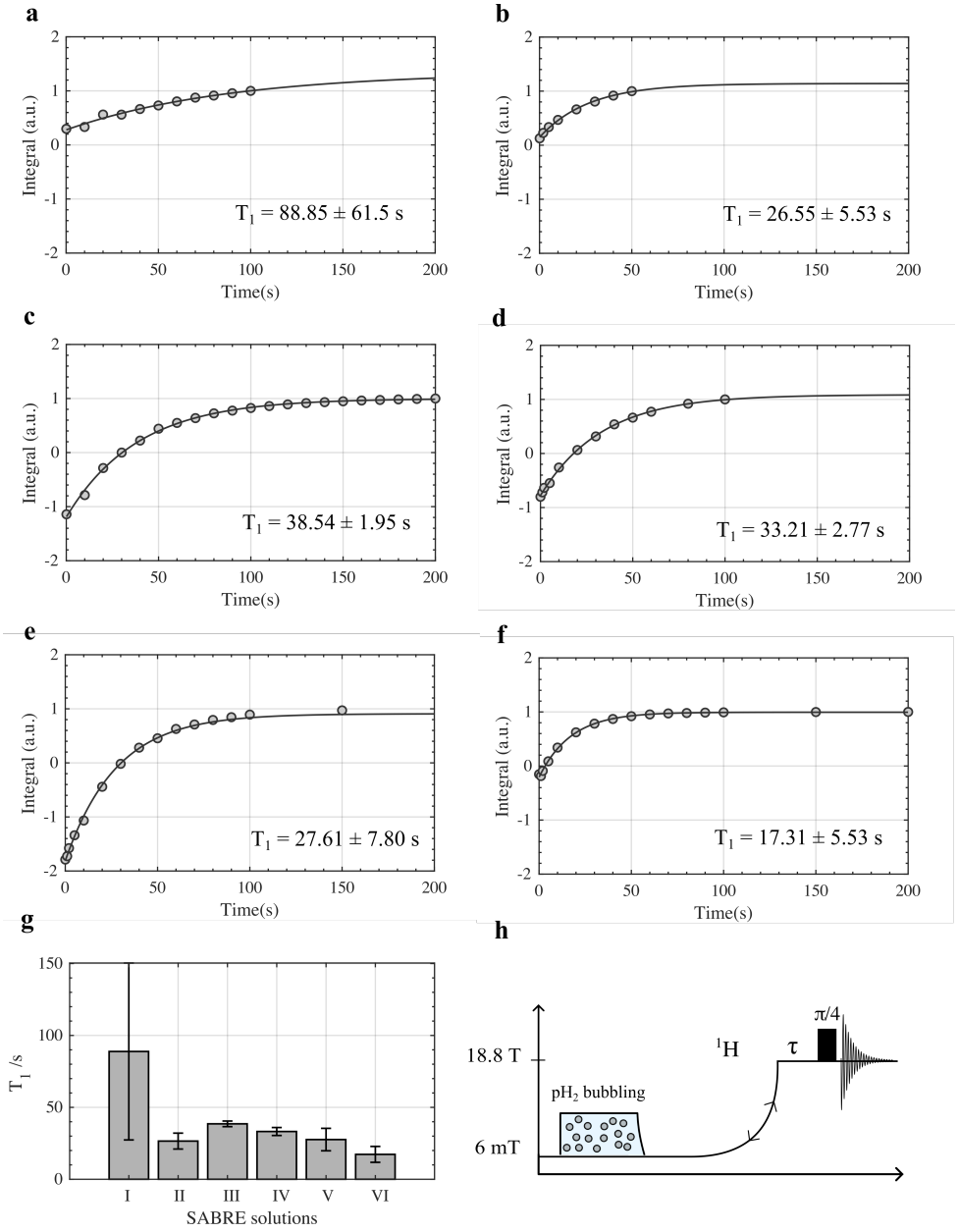

Figure S 14. Lifetime measurements of the solvent signal at 18.8 T in SABRE solutions I-VI displayed in respectively a-f). In g) the T_1 values are extracted using a mono-exponential buildup and plotted for all SABRE solutions. In h) the pulse sequence to extract the T_1 values is shown. A variable delay is used at high-field before measuring the solvent signal that has been subjected to 10 s of parahydrogen bubbling at a low-field of 6 mT. Note that for SABRE solutions I and II the polarization generated at low-field is positive due to cross-relaxation with pyridine,but is smaller than the thermal equilibrium polarization at 18.8 T. MATLAB is used for processing the data. The codes are available at https://doi.org/10.5281/zenodo.13952093.

9. References

1 O. Torres, M. Martín and E. Sola, Organometallics, 2009, 28, 863–870.

2 E. Vaneeckhaute, S. De Ridder, J.-M. Tyburn, J. G. Kempf, F. Taulelle, J. A. Martens and E. Breynaert, ChemPhysChem, 2021, 22, 1170–1177.

3 E. Rossini, A. D. Bochevarov and E. W. Knapp, ACS Omega, 2018, 3, 1653–1662.

4 J. A. Aguilar, P. I. P. Elliott, J. López-Serrano, R. W. Adams and S. B. Duckett, Chem. Commun., 2007, 1183–1185.

5 P. Kating, A. Wandelt, R. Selke and J. Bargon, J. Phys. Chem., 1993, 97, 13313–13317.

6 L. Sellies, I. Reile, R. L. E. G. Aspers, M. C. Feiters, F. P. J. T. Rutjes and M. Tessari, Chem. Commun., 2019, 55, 7235–7238.

7 S. Knecht, S. Hadjiali, D. A. Barskiy, A. Pines, G. Sauer, A. S. Kiryutin, K. L. Ivanov, A. V. Yurkovskaya and G. Buntkowsky, J. Phys. Chem. C, 2019, 123, 16288–16293.

8 E. Vaneeckhaute, J.-M. Tyburn, J. G. Kempf, J. A. Martens and E. Breynaert, J. Phys. Chem. Lett., 2022, 13, 3516–3522.

9 L. Dagys, M. C. Korzeczek, A. J. Parker, J. Eills, J. W. Blanchard, C. Bengs, M. H. Levitt, S. Knecht, I. Schwartz and M. B. Plenio, Sci. Adv., 2024, 10, eado0373.